Electrochemistry Communications 165 (2024) 107750

Contents lists available at ScienceDirect

Electrochemistry Communications

journal homepage: www.elsevier.com/locate/elecom

Full Communication

Evaluation of in-plane architecture in a thermo-electrochemical cell with nanostructured and porous Sb:SnO_2 electrodes

S. Castro-Ruiz, J. García-Cañadas *

Department of Industrial Systems Engineering and Design, Universitat Jaume I, Av. Vicent Sos Baynat s/n, 12006 Castelló de la Plana, Spain

ARTICLE INFO

Keywords:
Thermocell
Thermogalvanic cell
Impedance spectroscopy
Seebeck coefficient
Metal oxide

ABSTRACT

Thermo-electrochemical cells (TECs) are able to convert heat into electricity. They are formed by two electrodes (typically Pt) separated by a redox electrolyte (usually 0.4 M aqueous ferro/ferricyanide). The widely adopted architecture of TECs consists of the two electrodes separated by an electrolyte channel. To our knowledge, no studies have been reported exploring a different architecture. Here, we evaluate an alternative configuration, which comprises a substrate with the two electrodes at its ends and with the electrolyte added on the top contacting both electrodes, forming a planar configuration. We explore first the use of the standard Pt electrodes deposited on top of a conductive glass substrate. Then, we replace the Pt by nanostructured and porous Sb-doped SnO_2. The planar configurations are compared with their corresponding typical architectures using the common ferro/ferricyanide electrolyte. It was found that the planar TEC with Sb:SnO_2 reached a temperature coefficient of 1.76 mV/K, higher than the value obtained in the standard configuration with Sb:SnO_2 (1.21 mV/K), and also higher than the planar architecture with Pt electrodes, which showed the typical value for the ferro/ferricyanide electrolyte (1.45 mV/K). As a consequence of this significantly larger value, a 29.7 % higher maximum power output than the planar TEC with Pt was observed. Our study identifies for the first time interesting new features when a planar architecture is employed, opening the door to explore in more detail this alternative configuration in TECs.

1. Introduction

More than 60 % of the global energy consumed is lost as waste heat, being more than 80 % at low temperature (<100 °C) [1]. Only a 10 % recovery of this waste heat would exceed the summation of the current renewable energies [2]. On the other hand, different heat sources such as the sun or even our own bodies are widely spread and could provide enough amount of energy to power low-consumption sensors and wearable devices [3]. Hence, it would be highly beneficial to have a technology able to convert this vast amount of energy into electricity.

Thermo-electrochemical cells (TECs, or thermogalvanic cells or thermocells) are able to perform this by means of electrochemical processes [4]. They are formed by two electrodes separated by a redox electrolyte, which is typically a liquid or a gel. For this reason, they are intended for low temperature (<100 °C) applications [5,6]. Unlike conventional thermoelectrics, they show larger open-circuit potential vs temperature difference ratios, typically in the order of mV/K. The open-circuit potential in these cells rises due to the temperature dependency of the redox potential of the electrolyte (thermogalvanic effect) [7]. The benchmark TEC is formed by two Pt electrodes at different temperatures contacted by a 0.4 M ferro/ferricyanide aqueous redox electrolyte. This redox couple exhibits a temperature coefficient α of 1.40 mV/K [8].

The widely adopted architecture of TECs consists of the two electrodes separated by an electrolyte channel. Apart from this, U-shaped cells have also been reported casually [9,10], and other examples of different configurations can be found [11–13]. Here, we evaluate a different architecture, which comprises a substrate with the two electrodes at its ends and the electrolyte is added on the top contacting both electrodes, forming a planar configuration. In our study, we explore first the use of the standard Pt electrodes deposited on top of a conductive glass substrate. Then, we replace the Pt by nanostructured and porous Sb-doped SnO_2 (ATO), which has been recently reported to be a suitable electrode material in TECs [14]. The planar configurations are compared with their corresponding typical architectures using the common ferro/ferricyanide electrolyte. Interesting new features were found that encourage the further exploration of this architecture in TECs.

* Corresponding author.
E-mail address: garciaj@uji.es (J. García-Cañadas).

https://doi.org/10.1016/j.elecom.2024.107750
Received 24 March 2024; Received in revised form 6 May 2024; Accepted 9 May 2024
Available online 11 May 2024

2. Experimental section

Electrodes fabrication: Nanostructured and porous Sb:SnO_2 films were deposited on top of F-doped SnO_2 (FTO) glass substrates (Sigma Aldrich, 735167-EA) of 25 mm × 25 mm × 2.2 mm size, for the standard configuration, and 25 mm × 15 mm × 2.2 mm size for the in-plane case (see Fig. 1a). A previously described procedure was followed [15]. The substrates were cleaned before the ATO film deposition by means of three sonication steps of 15 min in different media. In the first step, sonication was performed using a soap (Labkem, SOAP-0685K0)/water solution (1:10 v/v). Then, distilled water to remove soap excess was used as second step. Finally, isopropanol (Labkem, PROL-P0P-5K0) media was employed for sonication. After this, substrates were dried under compressed air flow and treated in a UV-ozone cleaner (Ossila, L2002A2-UK) for 20 min. To avoid creating a short circuit in the planar configuration systems, two scratches were made on the FTO layer prior to the ATO deposition. These scratches were separated 3 mm, which is the separation distance between electrodes (see Fig. 1a, c and e). Subsequently, an Sb:SnO_2 colloidal aqueous dispersion (Keeling & Walker, A20W) was deposited by spin coating (Laurell, WS-650MZ-23NPPB) at 2500 rpm for 15 s, covering a centred area of the substrate of 15 mm × 15 mm, for the standard configurations, and the whole substrate, except the area that separates the electrodes, for the planar systems (see Fig. 1a). Five Sb:SnO_2 layers were deposited in all cases. After each layer deposition, a drying process was carried out on a hot plate at 100 °C for 10 min. Finally, the films were annealed at 550 °C for 45 min in a furnace (Nabertherm, 400-1) with a 3 °C/min heating rate. The morphology of the films was analysed by scanning electron microscopy (SEM) using a JEOL 7001F instrument (Oxford Instruments).

On the other hand, Pt electrodes were prepared by depositing Pt (target from Aname, SC502-314C) by sputtering (Quorum, Q300T D Plus) on the abovementioned cleaned FTO glasses during 6 min. The dimensions and location of the films were identical to the case of the ATO samples above, and the scratches to separate 3 mm the electrodes in the planar configuration samples were also performed (see Fig. 1a).

Apart from the ATO and Pt electrodes, a bare FTO glass was also tested for comparison, which was also scratched as discussed. All the electrodes employed can be seen in Fig. 1a.

Cells preparation: Three different symmetrical cells were prepared in the standard configuration. One of them using the FTO/ATO electrodes, another one with the Pt films deposited onto FTO glass, and the final one using only FTO glass. To improve the electrical contact in this configuration, a certain top area of the samples was painted with Ag paint (RS, 186–3600), as shown in Fig. 1a. In addition to the standard configuration cells, their corresponding planar versions were also prepared. In these cases, Ag paint was added at the ends of the electrodes and the 3 mm gap between electrodes was covered with tape to avoid contact with the electrolyte (see Fig. 1a, c and e). A solution of 0.4 M potassium ferrocyanide (Sigma Aldrich, P3289-100G) and 0.4 M potassium ferricyanide (Fluka, BCBT1564) in milli-Q water was employed as electrolyte in all the cells. All the chemicals were used as received.

Characterization setups: To characterize the TECs in standard configuration, a custom setup was employed (see Fig. 1b and d). In order to establish a temperature difference across the cell, two copper blocks were employed. One of them, with 30 mm × 30 mm × 10 mm dimensions and 2 cartridge heaters inserted (Watlow, C1A-9604), acted as the heat source. The heaters were powered using a Keithley 2601 source meter. A second larger copper block (Tangxi X00170O3IZ) of 40 mm × 40 mm × 10 mm dimensions with a water circulation channel was used as the heat sink. A water circulator (PolySicence, SD07R-20-A12E) served to circulate the water at a certain temperature along the Cu block.

The electrodes for each cell were centered on top of the copper blocks. Thermal grease (RS, 1938247) was used at all the glass/Cu interfaces to improve the thermal contacts. The electrodes were separated by a polytetrafluoroethylene (PTFE) piece which contained the electrolyte in a cylindrical channel of 10 mm length and 4 mm diameter. The channel connected to two top holes for the injection of the electrolyte. These holes were covered with tape after inserting the electrolyte to avoid evaporation.

To avoid electrolyte leakage, two O-rings of 8 mm internal diameter were located at the sides of the PTFE piece and were pressed against the electrodes by a system formed by stainless steel plates and screws. Two stainless steel screws inserted in the Cu blocks were used as electrical contacts for the current flow and two spring probes were contacted on top of the Cu blocks to sense the voltage (see Fig. 1b). The Cu blocks were electrically connected to the electrodes by Ag paint (see Fig. 1b).

On the other hand, a different setup was fabricated for the planar TECs. In order to establish the temperature difference in this setup, two metal blocks were employed. One of them made by Cu, with 30 mm × 30 mm × 10 mm dimensions and 3 cartridge heaters inserted (Watlow, C1A-9604), acted as the heat source. The heaters were also powered using a Keithley 2601 source meter. A second block made of Al of 30

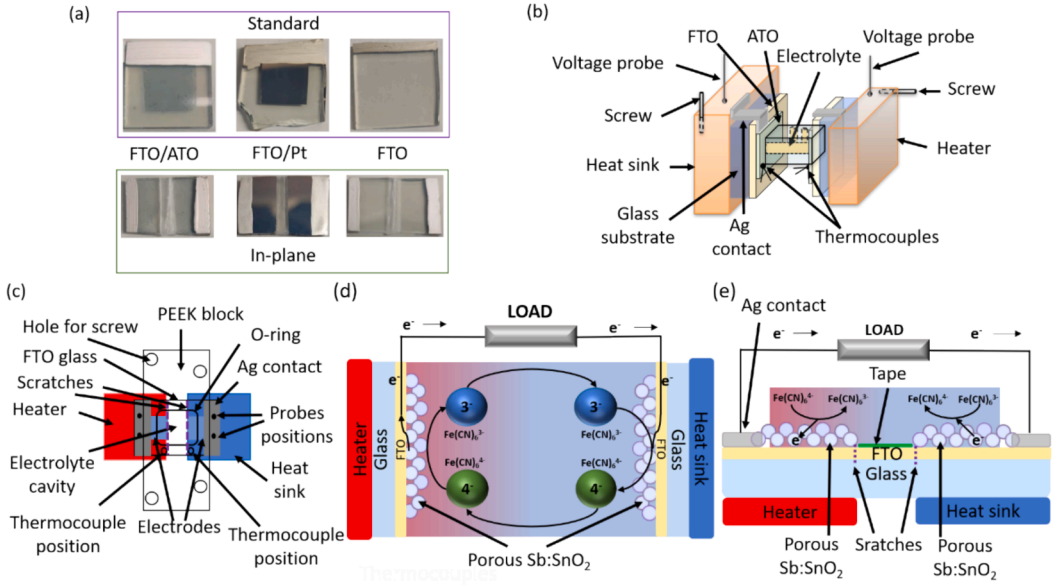

Fig. 1. (a) Different electrodes employed. Schemes of the (b, c) setups and (d, e) cells used, when Sb:SnO_2 was the electrode. (b, d) correspond to the standard configuration and (c, e) to the planar architecture (not to scale). (b) has been reprinted from ref. [14].

mm × 30 mm × 12 mm dimensions (Flyphant 30B3334A) with a water circulation channel was used as the heat sink. The same water circulator (PolySicence, SD07R-20-A12E) was employed to circulate the water at a certain temperature along this block. The FTO substrates with the electrodes were placed on top of the metal blocks, which were separated 3 mm by a PTFE bridge (see Fig. 1c). The latter helps to avoid breaking the sample during the time a pressure is applied by an O-ring to allocate the liquid electrolyte. Thermal grease (RS, 2173835) was used at the substrate/metal block interfaces to improve the thermal contacts. It should be noted that the bridge length is the same as the gap between the electrodes.

A holed polyetheretherketone (PEEK) block with a rectangular O-ring at the bottom side was placed on top of the glass substrate to allow the location of the electrolyte (see Fig. 1c). The location of the O-ring pressing the film can be seen in Fig. 1c. Once the electrolyte was added, a PTFE lid was placed to avoid evaporation. The PEEK block also has holes for positioning two thermocouples and several screws to provide a gentle pressure to avoid electrolyte leakage. The electric contacts to the external circuit were made with four spring probes (RS, 261–5092) contacting on the Ag contacts, as shown in Fig. 1c. The area of each electrode in contact with the electrolyte for this setup was 8.5 mm × 4.5 mm.

Measurements: The temperature coefficient α, was obtained from the slope of an open-circuit voltage V_{oc} vs the temperature difference ΔT plot. The V_{oc} was measured with a Keithley 2100 nanovoltmeter. The temperature difference was increased in steps of ≈2.5 K, from 0 up to ≈10 K, keeping the cold side temperature T_C fixed at 25.0 °C. To monitor the temperature, two K-type thermocouples (RS, 814–0134) and a dual thermometer (RS,123-2214) were employed. The thermocouples were positioned on top of the electrodes in the standard setup (see Fig. 1b) and on top of the substrate, aligned with the ends of the metal blocks (see Fig. 1c), in the planar system. In both cases, a bit of thermal grease was applied at their tips for thermalization.

To evaluate the performance of the TECs, impedance spectroscopy was used. Impedance measurements were carried out oscillating around the V_{oc} value when the cells were under a $\Delta T = 10$ K ($T_C = 25.0$ °C) using an amplitude of 15 mV in a frequency range from 1 MHz to 1 mHz. A Metrohm-Autolab PGSTAT302N potentiostat equipped with a FRA32M frequency response analyser controlled by Nova 1.11 software was used. ZView 3.5 h was employed to fit the experimental impedance results to different equivalent circuits.

3. Results and discussion

Fig. 2 shows SEM images of the ATO film employed. It can be seen that the film is formed by interconnected nanoparticles of sizes below 10 nm. Moreover, pores are present with sizes not larger than around 30 nm (see inset of Fig. 2a). A thickness value of 550 nm was estimated from the cross-sectional image (Fig. 2b). It should be noted that the expected phase (cassiterite SnO_2) was previously identified by XRD experiments in our previous article [15]. Also, it can be seen in that reference that no changes in the XRD patterns were observed after the annealing process. Similarly, an EDX analysis from the same article showed no changes in the chemical composition of the film after the thermal treatment.

Fig. 3 shows the impedance results obtained for each cell with their corresponding fittings, performed using the equivalent circuits shown in the inset [14,16]. The fitted parameters with their corresponding errors are shown in Table 1. On the one hand, for the TECs with the ATO and Pt electrodes, either in standard or planar configuration, an equivalent circuit formed by a series resistance R_s (accounting for the cables, contacts and electrolyte resistances) and the finite-length Warburg impedance with a transmissive boundary (short-circuit terminus W_s), both connected in series, was used (see inset of Fig. 3a). The impedance of the W_s element is defined as $Z_{Ws} = R_{mt}(j\omega d^2/D)^{-p} \tanh[(j\omega d^2/D)^p]$, being R_{mt} the mass-transport resistance, related to the diffusion of the redox species to/from the electrodes, $j=(-1)^{0.5}$, ω the angular frequency, d the diffusion length, D the diffusion coefficient of the redox species (assumed equal for both molecules), and p an exponent, which accounts for deviations from the ideal value ($p = 0.5$) [17,18].

On the other hand, when bare FTO glasses were used as electrodes two new elements in the equivalent circuit, a charge-transfer resistance R_{ct}, related to the kinetics of the transfer of electrons between the redox species and the electrodes, and a double-layer capacitor, accounting for the accumulation of charge at the electrode/electrolyte interface, were added to the previous equivalent circuit (see inset of Fig. 3b). These two elements (R_{ct} and C_{dl}) produce the semicircle observed at the left part in the Nyquist plots (see Fig. 3) [19]. In the case of the ATO and Pt electrodes, this semicircle does not appear, indicating good redox kinetics, as previously reported by our group [14].

From the impedance analysis (Table 1), the different processes that govern the performance of the cells can be identified. First, it can be seen that the R_s values are similar within each configuration, which is expected since the electrolyte and dimensions of the different cell elements are similar. When comparing both configurations, a higher R_s value is found for the standard case, which we attribute to a larger electrolyte resistance due to the higher separation between electrodes (10 mm in the standard case vs 3 mm in the planar configuration).

Regarding the mass transport, R_{mt} values are again similar within the cells of each configuration, as expected, since the same electrolyte is used. However, this is not the case for the system with ATO electrodes in in-plane configuration, which shows a R_{mt} value around 7 Ω higher than the other two planar cells. This could be due to the somewhat more difficult diffusion of the redox species within the nanostructured and

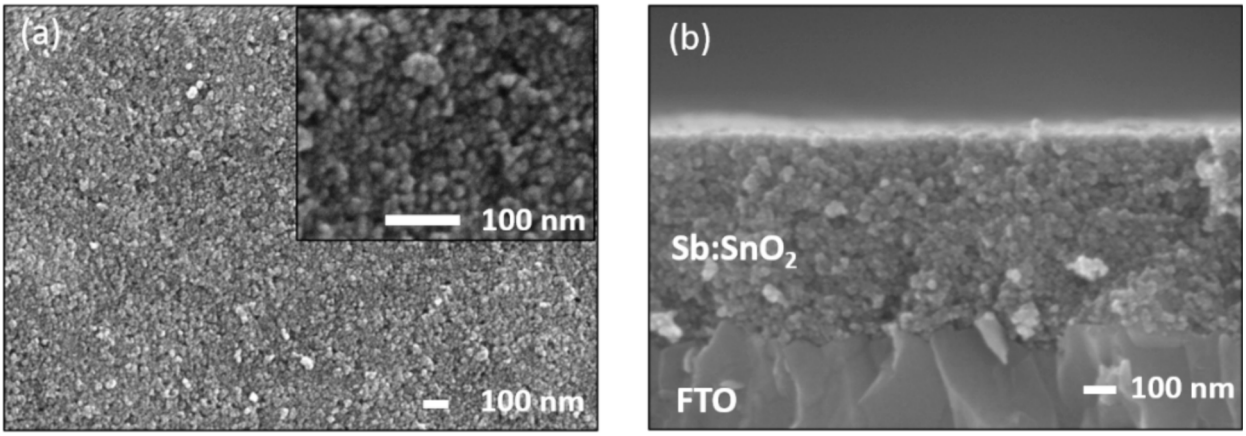

Fig. 2. (a) Top and (b) cross-sectional SEM images of an Sb:SnO_2 film prepared (reprinted from ref. [14]).

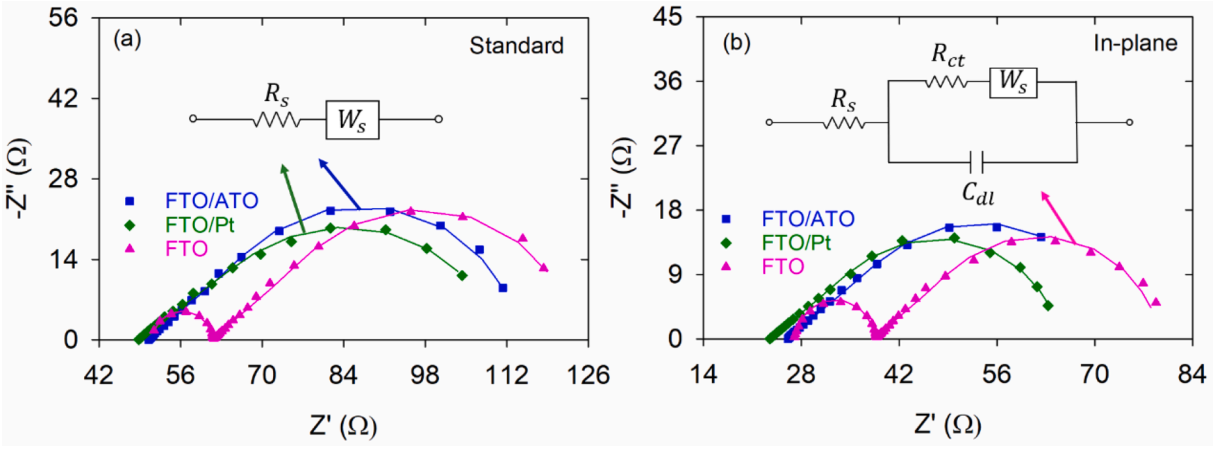

Fig. 3. Impedance spectra (Nyquist plots) for the cells in (a) standard and (b) in-plane configurations with Sb:SnO_2 (blue), Pt (green) and bare FTO (pink) electrodes. The lines correspond to the fittings performed. (For interpretation of the references to colour in this figure legend, the reader is referred to the web version of this article.)

Table 1
Temperature coefficient (α), series (R_s) and charge-transfer (R_{ct}) resistances, double-layer capacitance (C_{dl}), mass-transfer resistance (R_{mt}), exponent (p) and R_{dc} of the different thermo-electrochemical cells in both horizontal and in-plane configurations when $\Delta T = 10$ K. Relative errors are shown between brackets. The maximum power output (P_{max}) is also indicated.

	Electrodes	α (mV/K)	R_s (Ω)	R_{ct} (Ω)	C_{dl}(μF)	R_{mt} (Ω)	p	R_{dc} (Ω)	P_{max} (μW)
Standard	FTO/ATO	1.21(0.89 %)	50.3(0.10 %)	–	–	64.0(0.53 %)	0.459(0.48 %)	114	0.321
	FTO/Pt	1.46(0.19 %)	48.4(0.17 %)	–	–	62.5(0.98 %)	0.408(0.49 %)	111	0.480
	FTO	1.29(0.13 %)	51.2(0.32 %)	10.0(1.73 %)	0.603(4.59 %)	62.5(0.97 %)	0.455(0.83 %)	124	0.335
In-plane	FTO/ATO	1.76(0.41 %)	25.9 (0.14 %)	–	–	48.3 (0.85 %)	0.430 (0.59 %)	74	1.05
	FTO/Pt	1.45(0.29 %)	23.4(0.11 %)	–	–	41.8(0.44 %)	0.428(0.42 %)	65	0.809
	FTO	1.42(0.22 %)	27.3(0.28 %)	11.0(0.88 %)	0.493(2.52 %)	41.1(0.90 %)	0.442(0.94 %)	79	0.638

porous morphology of the electrodes in the direction parallel to the substrate. In the standard configuration, the diffusion basically takes place in the direction perpendicular to the electrode. When comparing both configurations, again higher R_{mt} values are observed for the standard case (see Table 1), which we also attribute to the larger inter-electrode distance.

If we analyse now the different temperature coefficient values shown in Table 1, a significantly higher value of 1.76 mV/K was measured for the ATO system in planar configuration, which is 21.4 % higher than the value found for the cell with Pt electrodes in the same configuration (1.45 mV/K), which is in agreement with the standard value reported for this electrolyte (1.40 mV/K). Although we cannot find a clear explanation for this significant increase at this stage, we think that it might be related to the restrictions that the redox species can find when located within the intricated porous structure of the ATO film. In the standard configuration, where the temperature coefficient was 1.21 mV/K, the

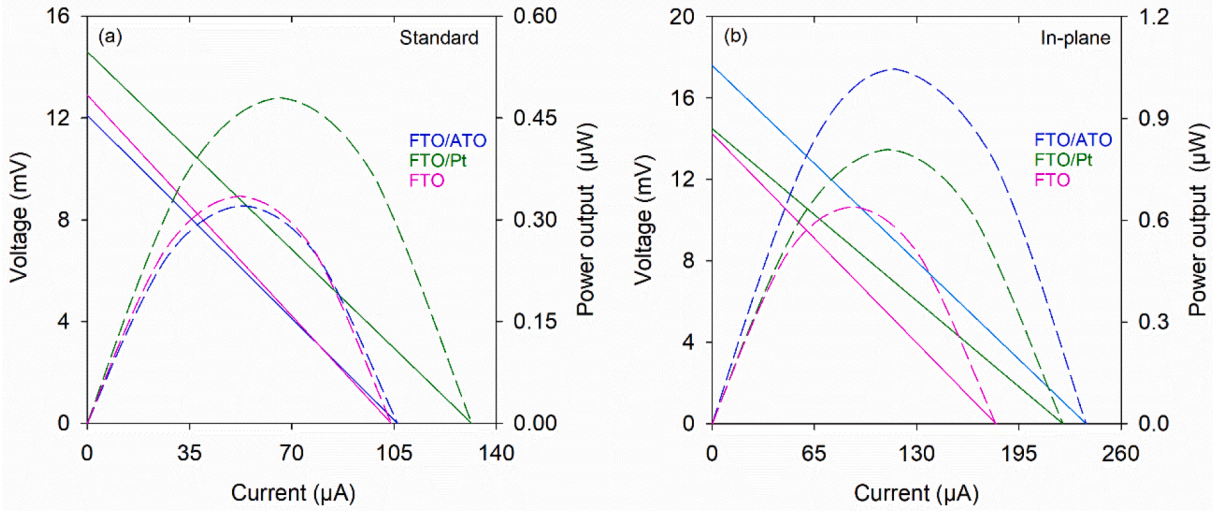

Fig. 4. Current-voltage (solid lines) and power output-current (dashed lines) curves under a 10 K temperature difference (cold side temperature kept fixed at 25 °C) for the cells with the Sb:SnO_2 films, the Pt electrodes, and the FTO-only cell in both configurations.

length of the diffusion path of the species within the ATO electrode is very short, since the film thickness is 550 nm. However, due to the change in orientation, in the planar configuration the diffusion paths can reach a few mm (electrodes length is 4.5 mm) when moving in the direction parallel to the substrate, which is a much higher value. This suggestion is in agreement with the higher R_{mt} value found discussed above. In any case, further studies will be conducted to try to explain in more detail this new effect observed.

In order to analyse the performance of the different cells, the current–voltage *I-V* curves [20] and the power output were obtained at $\Delta T = 10$ K (see Fig. 4). For the determination of the *I-V* curves the values of the V_{oc} and the dc resistance R_{dc} were considered. This dc resistance was extracted from the impedance results (see Table 1) and comprises the addition of all the different resistances identified in the impedance analysis ($R_{dc} = R_s + R_{ct} + R_{mt}$). This method to obtain the *I-V* curves has been validated [16] and also employed [14] by us previously. Its validity relies in the fact that the dc resistance governs the slope of the *I-V* curve [14,16]. Hence, if the open-circuit voltage ($V_{oc} = \alpha\Delta T$) and R_{dc} are known, the *I-V* curves and the maximum power [$P_{max} = {V_{oc}}^2/(4R_{dc})$] can be obtained (Fig. 4 and Table 1). When comparing the cells in planar configuration, it can be observed that a 29.7 % higher P_{max} can be reached in the ATO cell than in the Pt case. This is due to the larger temperature coefficient, despite having a somewhat higher R_{mt}.

It should be noticed that larger P_{max} values were obtained in all the in-plane systems when compared to their corresponding standard cells. However, this is not a fair comparison since the dimensions of both systems differ and the transport of the redox species is not exclusively one-dimensional in the in-plane architecture, as it is in the standard case.

4. Conclusions

An analysis of a new architecture for a thermo-electrochemical cell has been performed. Unlike the standard configuration where a redox electrolyte is sandwiched by two similar electrodes (typically Pt), the new architecture comprises a substrate (FTO glass) with the two electrodes deposited at its ends and the 0.4 M aqueous ferro/ferricyanide electrolyte added on the top contacting both electrodes, forming a planar configuration. Different cells were prepared using Pt films and nanostructured and porous Sb-doped SnO_2 electrodes in both architectures (standard and in-plane). Interestingly, a significantly higher temperature coefficient was found for the in-plane configuration when Sb:SnO_2 was used as electrode (1.76 mV/K), higher than the value obtained in the standard configuration with Sb:SnO_2 (1.21 mV/K), and also higher than the planar architecture with Pt electrodes, which showed the typical value for the ferro/ferricyanide electrolyte (1.45 mV/K). An analysis of these systems by impedance spectroscopy revealed that the main difference between the cells with planar configuration relies on a somewhat higher mass-transport resistance found for the Sb:SnO_2 system. In any case, the temperature coefficient improvement was more relevant and the maximum power output for the in-plane Sb:SnO_2 cell was 29.7 % higher than when using the typical Pt electrodes. Our study identifies for the first time interesting new features when a planar architecture is employed, opening the door to explore in more detail this alternative configuration.

CRediT authorship contribution statement

S. Castro-Ruiz: Writing – original draft, Visualization, Validation, Methodology, Investigation, Formal analysis. **J. García-Cañadas:** Writing – review & editing, Visualization, Supervision, Resources, Project administration, Methodology, Funding acquisition, Formal analysis, Conceptualization.

Declaration of competing interest

The authors declare that they have no known competing financial interests or personal relationships that could have appeared to influence the work reported in this paper.

Data availability

The data of this article can be obtained from the Zenodo repository

Acknowledgements

This project has received funding from the European Union's Horizon 2020 research and innovation programme under grant agreement No 863222 (UncorrelaTEd project).

References

[1] International Energy Agency. World Energy Outlook. 2023.
[2] Renewable Energy Agency I. Renewable Power Generation Costs in 2022. 2023.
[3] O. Farhat, J. Faraj, F. Hachem, C. Castelain, M. Khaled, A recent review on waste heat recovery methodologies and applications: Comprehensive review, critical analysis and potential recommendations, Clean. Eng. Technol. 6 (2022) 100387–100409, https://doi.org/10.1016/j.clet.2021.100387.
[4] Y. Liu, M. Cui, W. Ling, L. Cheng, H. Lei, W. Li, et al., Thermo-electrochemical cells for heat to electricity conversion: from mechanisms, materials, strategies to applications, Energ. Environ. Sci. 15 (2022) 3670–3687, https://doi.org/10.1039/d2ee01457b.
[5] W. Li, J. Ma, J. Qiu, S. Wang, Thermocells-enabled low-grade heat harvesting: challenge, progress, and prospects, Mater. Today Energy 27 (2022) 101032–110150, https://doi.org/10.1016/j.mtener.2022.101032.
[6] J. Duan, B. Yu, L. Huang, B. Hu, M. Xu, G. Feng, et al., Liquid-state thermocells: Opportunities and challenges for low-grade heat harvesting, Joule 5 (2021) 768–779, https://doi.org/10.1016/j.joule.2021.02.009.
[7] X. Qian, Z. Ma, Q. Huang, H. Jiang, R. Yang, Thermodynamics of Ionic Thermoelectrics for Low-Grade Heat Harvesting, ACS Energy Lett. (2024) 679–706, https://doi.org/10.1021/acsenergylett.3c02448.
[8] M.F. Dupont, D.R. MacFarlane, J.M. Pringle, Thermo-electrochemical cells for waste heat harvesting-progress and perspectives, Chem. Commun. 53 (2017) 6288–6302, https://doi.org/10.1039/c7cc02160g.
[9] D. Dong, H. Guo, G. Li, L. Yan, X. Zhang, W. Song, Assembling hollow carbon sphere-graphene polylithic aerogels for thermoelectric cells, Nano Energy 39 (2017) 470–477, https://doi.org/10.1016/j.nanoen.2017.07.029.
[10] W. Qian, M. Cao, F. Xie, C. Dong, Thermo-Electrochemical Cells Based on Carbon Nanotube Electrodes by Electrophoretic Deposition, Nanomicro Lett 8 (2016) 240–246, https://doi.org/10.1007/s40820-016-0082-8.
[11] M.S. Romano, N. Li, D. Antiohos, J.M. Razal, A. Nattestad, S. Beirne, et al., Carbon nanotube-reduced graphene oxide composites for thermal energy harvesting applications, Adv. Mater. 25 (2013) 6602–6606, https://doi.org/10.1002/adma.201303295.
[12] L. Yang, H. Sun, S. Wang, L. Jiang, G. Sun, A solid state thermogalvanic cell harvesting low-grade thermal energy, Int. J. Hydrogen Energy 42 (2017) 25877–25881, https://doi.org/10.1016/j.ijhydene.2017.08.111.
[13] Clampitt BH, German DE. Electrochemical cell for conversion of heat energy. US3253955A, 1966.
[14] S. Castro-Ruiz, J. García-Cañadas, Nanostructured and porous antimony-doped tin oxide as electrode material for the heat-to-electricity energy conversion in thermo-electrochemical cells, Electrochem. Commun. 161 (2024) 107683–107689, https://doi.org/10.1016/j.elecom.2024.107683.
[15] S. Castro-Ruiz, L. Márquez-García, M. Solis-De la Fuente, B. Beltrán-Pitarch, A. Mota-Babiloni, F. Vidan, et al., Power factor improvement in a solid-liquid thermoelectric system formed by Sb:SnO2 in contact with a chromium complex solution, Sustain Energy Fuels 7 (2023) 4254–4259, https://doi.org/10.1039/d3se00622k.
[16] S. Castro-Ruiz, J. García-Cañadas, Impedance spectroscopy analysis of a thermo-electrochemical cell under operating conditions, in: 2022 International Workshop on Impedance Spectroscopy (IWIS), 2022, pp. 25–27, 10.1109/IWIS57888.2022.9975126.
[17] A.C. Lazanas, M.I. Prodromidis, Electrochemical impedance spectroscopy-A tutorial, ACS Measur. Sci. Au 3 (2023) 162–193, https://doi.org/10.1021/acsmeasuresciau.2c00070.
[18] A. Lasia, Electrochemical Impedance Spectroscopy And Its Applications, Springer, New York, 2014, 10.1007/978-1-4614-8933-7.
[19] P. Yang, H. Fan, Electrochemical impedance analysis of thermogalvanic cells, Chem. Res. Chin. Univ. 36 (2020) 420–424, https://doi.org/10.1007/s40242-020-0126-y.
[20] M.A. Buckingham, L. Aldous, Thermogalvanic cells: A side-by-side comparison of measurement methods, J. Electroanal. Chem. 872 (2020) 114280–114290, https://doi.org/10.1016/j.jelechem.2020.114280.